Received: 30 September 2020 | Revised: 21 April 2021 | Accepted: 1 June 2021

DOI: 10.1002/pip.3443

RESEARCH ARTICLE

PROGRESS IN PHOTOVOLTAICS WILEY

Very thin crystalline silicon cells: A way to improve the photovoltaic performance at elevated temperatures

Hitoshi Sai | Yoshiki Sato | Toshiki Oku | Takuya Matsui

Global Zero Emission Research Center (GZR), National Institute of Advanced Industrial Science and Technology (AIST), Tsukuba, Ibrakaki, Japan

Correspondence
Hitoshi Sai, Global Zero Emission Research Center (GZR), National Institute of Advanced Industrial Science and Technology (AIST), Tsukuba, Ibrakaki 305-8568, Japan.
Email: hitoshi-sai@aist.go.jp

Abstract

In general, the conversion efficiency of solar cells decreases with the increase in temperature. This temperature dependence is mitigated by enhancing the open circuit voltage (V_{OC}). Given a solar cell, its V_{OC} can be enhanced by several routes, for example, reducing the defect density within the absorber, applying passivating contacts, and reducing the absorber thickness. In this work, we investigate the impact of wafer thickness in crystalline silicon (c-Si) solar cells from the viewpoint of the photovoltaic performance at elevated temperatures. It is confirmed experimentally that the V_{OC} of c-Si solar cells increases by thinning the Si wafer, for example, $V_{OC} \geq 0.75$ V is obtained at a wafer thickness of <60 μm with a conversion efficiency of 22.7%, if surface recombination is sufficiently suppressed. It is also confirmed that thin c-Si cells exhibiting high V_{OC} show less temperature dependence. As a result, the optimum wafer thickness for maximizing the efficiency decreases with the increase in temperature according to the relation of -1.1 μm/°C. Numerical simulation predicts that this tendency becomes more emphasized with the suppression of Shockley–Read–Hall recombination. These findings suggest that the device structure of c-Si solar cells including the choice of the wafer thickness should be optimized depending on the operating temperature in the field.

KEYWORDS

amorphous silicon, crystalline silicon, heterojunction, temperature, temperature coefficien0074, thickness, thin

1 | INTRODUCTION

It has been recognized that photovoltaics (PV) is one of the most reliable and cost-effective renewable energy sources for electricity. PV already covered approximately 3% of the world's electricity generation in 2019,[1] and further penetration is highly expected to realize the low carbon society and slow down the global warming. In general, the performance of solar cells is quantified and compared based on the conversion efficiency, which is normally determined under standard test conditions (STC; solar irradiation of 100 mW cm^{-2}, air mass 1.5 global, and a temperature of 25°C). However, the actual operating conditions in the field significantly deviate from STC. For example, the temperature of PV modules can be higher by 30°C or more than the ambient temperature, according to the conditions.[2–5] The performance of PV modules inevitably degrades with the increase in temperature,[6] because the intrinsic carrier density increases exponentially with temperature rising, resulting in the drastic increase in the saturation current density and the reduction in open circuit voltage (V_{OC}). Therefore, it is crucial to minimize the temperature dependence as well as to improve the conversion efficiency under STC. In general, temperature dependence of a solar cell is quantified with the temperature coefficient (TC) of the conversion efficiency (TC_η). TC_η is the sum of the TCs of the photovoltaic parameters as[7]

$$TC_\eta = TC_{VOC} + TC_{JSC} + TC_{FF}, \quad (1)$$

where TC_{VOC}, TC_{JSC}, and TC_{FF} are the TCs of the V_{OC}, the short-circuit current density (J_{SC}), and the fill factor (FF), respectively. The TC_η of a solar cell is closely linked with its V_{OC} (and hence TC_{VOC}) which is the most sensitive to temperature variation among these parameters.

In recent years, crystalline silicon (c-Si) solar cells have dominated the PV market, and their V_{OC} has been steadily improved from ~0.60 to > 0.70 V by adapting the more advanced cell architectures with better surface passivation including passivating contact technologies. Currently, the most successful passivating contacts are realized by very thin tunnel oxide (called as TOPCon[8] or POLO[9]) or amorphous silicon (silicon heterojunction, SHJ[10]) films. The record-efficiency cell with the TOPCon structure shows a V_{OC} of 0.732 V and an efficiency of 26.0% in the area of 4 cm^2,[11] while that of the SHJ technology exhibits a notably high V_{OC} of 0.747 V and an efficiency of 25.1% in a full-size 6-inch wafer.[12] In fact, it was reported that c-Si cells with these advanced architecture show better TCs owing to their high V_{OC}.[13–15]

A pathway to improve the V_{OC} further in high-efficiency c-Si cells is to thin down the Si wafer. In general, the V_{OC} of c-Si solar cells increases with the decrease in wafer thickness via enlarging the ratio of the photocurrent density over the saturation current density.[15] This concept was already investigated with SHJ solar cells by several groups,[16–20] and high V_{OC} exceeding 0.75 V was confirmed experimentally.[17,21,22] In contrast, the thinner the wafer becomes, the smaller short-circuit current density (J_{SC}) is obtained, as a result of the volume reduction of the c-Si absorber. Accordingly, an optimum wafer thickness exists in terms of the conversion efficiency owing to the trade-off relationship between the V_{OC} and the J_{SC}. The optimum wafer thickness at room temperature is approximately 98–110 μm for the ideal case,[23,24] and it can be thinner for the case that the efficiency is limited by the material quality.[25] In principle, the optimum wafer thickness is supposed to be dependent on the operating temperature, as the advantage of having a high V_{OC} becomes more significant at elevated temperatures. This idea is supported by Engelbrecht and Tiedje in their very recent work based on limiting efficiency calculation.[26] However, there is no clear experimental evidence on this issue and further research is needed. Another benefit of high-V_{OC} cells is the increase of the operating voltage at the maximum power point (V_{MPP}) in the field. It is known that c-Si cells with higher V_{MPP} lead to a better TC_η in PV modules, since they reduce the relative impact of the additional electrical losses, for example, resistance loss due to interconnections.[14]

In this work, we investigate the impact of wafer thickness on the TC in c-Si solar cells from both sides of experiment and calculation. A series of SHJ solar cells with a wide range of thicknesses from 50 to 400 μm is prepared as a testbed of high-V_{OC} c-Si cells, and their photovoltaic properties are characterized at various temperatures. It is confirmed that the TC of the efficiency is improved by increasing the V_{OC} via either improving surface passivation or thinning the c-Si wafer in SHJ solar cells. We also discuss the impact of temperature on the optimum wafer thickness in c-Si cells with the help of numerical simulation.

2 | EXPERIMENTAL

2.1 | Solar cell fabrication

The structure of SHJ solar cells fabricated in this study is schematically shown in Figure 1. We used P-doped *n*-type Czochralski (CZ)-grown monocrystalline Si wafers (~2 Ωcm, <100>-oriented) as substrates, and their thicknesses were varied from 50 to 400 μm by means of mechanical thinning and polishing. Then the wafers were cut into small pieces with a size of 50 mm × 50 mm because of the size limitation in our experimental facilities, followed by surface texturing with KOH-based wet etching (Hayashi Pure Chemical, Pure Tech) to form random pyramids on both surfaces. The average thickness (w) of each wafer was determined by measuring their weight with an accuracy of ± 0.5 μm. After wet-chemical cleaning with our standard cleaning process,[27] intrinsic (i) and doped (*p*- and *n*-type) thin hydrogenated amorphous silicon (a-Si:H) layers were successively deposited on the both sides of the textured wafers by means of plasma-enhanced chemical vapor deposition (PECVD). The detail condition of our PECVD process was reported elsewhere.[19,28,29] In this study, we prepared two different groups of SHJ solar cells by controlling the deposition condition of (i)a-Si:H in terms of surface passivation, that is, the samples with our standard deposition condition (Group A) and those with intentionally deteriorated surface passivation and therefore lower conversion efficiencies (Group B). After the PECVD process, In_2O_3:Sn (ITO) films and Ag electrodes were formed on both sides of the precursor by means of magnetron sputtering with shadow masks. Thermal annealing was performed at 160°C after the ITO depositions to recover the lifetime degradation during sputtering.

2.2 | Characterization

The effective minority carrier lifetimes (τ_{eff}) of the SHJ cell precursors were monitored at each process step with Quasi-Steady-State

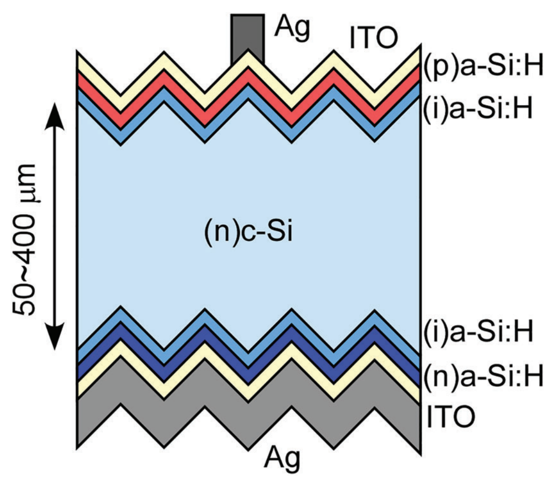

FIGURE 1 Schematic illustration of the SHJ solar cell fabricated in this study [Colour figure can be viewed at wileyonlinelibrary.com]

Photo-Conductance (QSSPC) measurement setup (Sinton Instruments, WCT-120). In this work, τ_{eff} was characterized for the SHJ cells with a wide range of w. Therefore, the bulk lifetime (τ_{bulk}) and the surface recombination velocity (S) can be determined by the following relationship.[30]

$$\frac{1}{\tau_{eff}} = \frac{1}{\tau_{bulk}} + \frac{2S}{w}. \tag{2}$$

Here, we determine S by using SHJ solar cells which have two different interfaces (pi- and ni-sides) with surface textures, so that the experimentally determined S is regarded as the mean surface recombination velocity (S_{mean}).

The current density-voltage (J-V) characteristics of the SHJ cell were evaluated using a solar simulator under STC condition using a class A solar simulator (Wacom), and the V_{OC}, J_{SC}, FF, and η were recorded. The cell area was 4 cm^2 designated by a shadow mask during the measurement. Light intensity-dependent V_{OC} measurement (suns-V_{OC}) was also performed with the shadow mask to extract the pseudo FF (pFF), which is the maximum achievable FF when the series resistance is negligible.[31]

Temperature-dependent J-V characteristics of the SHJ solar cells were also measured by using a temperature-controlled chamber with a solar simulator. The sample temperature (T) was varied from room temperature to approximately 60°C and monitored with a thermocouple attached directly on a dummy SHJ cell, which was fixed adjacent to the sample. With the measured T-dependent J-V parameters, the TC_{VOC}, the TC_{JSC}, the TC_{FF}, and the TC_{η} are calculated by

$$TC_{VOC} = \frac{1}{V_{OC,25^{\circ}C}} \frac{dV_{OC}}{dT}, \tag{3}$$

$$TC_{JSC} = \frac{1}{J_{SC,25^{\circ}C}} \frac{dJ_{SC}}{dT}, \tag{4}$$

$$TC_{FF} = \frac{1}{FF_{25^{\circ}C}} \frac{dFF}{dT}, \tag{5}$$

$$TC_{\eta} = \frac{1}{\eta_{25^{\circ}C}} \frac{d\eta}{dT}. \tag{6}$$

Thus, TCs are normalized by the corresponding parameters at 25°C in this study.

3 | SIMULATION

3.1 | Calculation of implied *J-V* characteristics

In this study, the implied J-V characteristics is analyzed by numerical calculations to assess the impact of the device temperature and the wafer thickness on the photovoltaic performance in ideal c-Si cells. In the following, we briefly describe the basic formulae for simulating the implied J-V characteristics.[17,19,32]

The iV_{OC} of a solar cell is calculated by

$$iV_{OC}(\Delta n) = \frac{kT}{q} ln\left\{\frac{(n_0+\Delta n)(p_0+\Delta p)}{n_i^2}\right\} \tag{7}$$

where k is the Boltzmann constant, q is the elementary charge, n_0 (p_0), and Δn (Δp) are the equilibrium and the excess concentrations of electrons (holes), respectively, and n_i is the intrinsic carrier density. The recombination current density (J_{rec}) can be written as

$$J_{rec}(\Delta n) = qw\frac{\Delta n}{\tau_{eff}}, \tag{8}$$

where τ_{eff} is again the effective lifetime. The implied J-V curves are derived for a range of Δn, by combining Equations 7 and 8. τ_{eff} is given by

$$\begin{aligned} \tau_{eff} &= \left(\frac{1}{\tau_{rad}} + \frac{1}{\tau_{Auger}} + \frac{1}{\tau_{SRH,bulk}} + \frac{1}{\tau_{surf}}\right)^{-1} \\ &= \left(\frac{1}{\tau_{int}} + \frac{1}{\tau_{SRH,bulk}} + \frac{1}{\tau_{surf}}\right)^{-1} \\ &= \left(\frac{1}{\tau_{bulk}} + \frac{1}{\tau_{surf}}\right)^{-1}, \end{aligned} \tag{9}$$

where τ_{rad}, τ_{Auger}, and $\tau_{SRH,bulk}$ are the lifetimes due to bulk radiative, Auger, and Shockley–Read–Hall (SRH) recombination, respectively, and τ_{surf} is the lifetime due to the surface recombination. Here, the intrinsic lifetime τ_{int} is defined as the lifetime due to τ_{rad} and τ_{Auger}, while τ_{bulk} is the lifetime determined by all the bulk recombination processes. τ_{surf} is given by

$$\tau_{surf} = \frac{\Delta n \cdot w}{2R_{surf}}, \tag{10}$$

where R_{surf} is the surface recombination rate and linked with S by the relation

$$S = R_{surf}/\Delta n. \tag{11}$$

In a solar cell under steady-state illumination, the photocurrent density (J_{photo}) is given by

$$J_{photo} = iJ_{SC} - J_{rec}(\Delta n), \tag{12}$$

where iJ_{SC} is the implied J_{SC}. Here, we calculate iJ_{SC} by assuming the ideal Lambertian light trapping.[33] Equation 12 gives the illuminated implied J-V curves and allows to calculate implied FF (iFF).

In this study, we consider only n-type Si wafers with $n_0 = 2.4 \times 10^{15}$ cm^{-3}, which corresponds to the doping concentration of the Si wafers used in this work (2 Ωcm).

3.2 | Temperature dependence

Temperature change affects on many aspects of the light absorption and the charge carrier behavior within c-Si solar cells. In this work, we consider the following parameters as T dependent: (i) energy gap E_g, (ii) optical absorption coefficient, (iii) intrinsic carrier density n_i.

i. Energy bandgap E_g

In general, the bandgap energy E_g decreases with increasing T (bandgap narrowing). In this study, the T-dependent energy bandgap of c-Si, $E_g(T)$, is calculated by using Pässler's model.[34] Note that $E_g(T)$ decreases almost linearly with the increase in T in the temperature range considered in this study (T > 250 K).[35]

ii. Optical absorption

Optical absorption in c-Si is dependent on T owing to the bandgap narrowing, particularly for the wavelengths near E_g. This must be taken into consideration for calculating the iJ_{SC} at various temperatures. Here, we use the self-consistent optical constants of intrinsic c-Si and their temperature coefficient reported by Green.[36] More recently, Nguyen et al[37] also reported T-dependent band-to-band absorption coefficient based on photoluminescence measurement, which agrees well with Green's data.

iii. Intrinsic carrier density n_i

n_i is a crucial parameter for the determination of carrier recombination, and defined by the equilibrium electron and hole concentration as[15,35]

$$n_i(T)^2 = N_C(T)N_V(T)exp\left(-\frac{E_g(T)}{kT}\right). \tag{13}$$

Thus, n_i^2 depends on $E_g(T)/T$ exponentially. Here, N_C and N_V are the effective densities of states of conduction and valence bands, respectively, and are defined as

$$N_C(T) = 2\left(\frac{2\pi m^*_{dc}(T)kT}{h^2}\right)^{\frac{3}{2}}, \tag{14}$$

$$N_V(T) = 2\left(\frac{2\pi m^*_{dv}(T)kT}{h^2}\right)^{\frac{3}{2}}, \tag{15}$$

where m^*_{dc} and m^*_{dv} are the density-of-states effective masses in the conduction and valence bands, respectively, and h is Planck's constant. T dependences of m^*_{dc} and m^*_{dv} are originated from the electronic band structure of c-Si near the bandgap (the conduction band minima and the valence band maxima).[35] In this study, we apply the parameterization reported by Couderc et al[38] for calculating $m^*_{dc}(T)$ and $m^*_{dv}(T)$ and hence $n_i(T)$.

In general, recombination parameters are dependent on T. It is known that T dependences of radiative[39,40] and Auger recombination[41] are weak in the T-range considered in this study. Therefore, we herein use the most accurate Richter parameterization[42] for calculating τ_{int}, though it is determined for 300 K and does not include T dependence explicitly.

In contrast, T dependences of bulk and surface SRH recombination is more complex, because it depends on the type of the relevant recombination center (carrier trap state) with multiple parameters (density, energy level, capture cross sections, etc.).[43–46] T dependence of the τ_{eff} in SHJ cells, which are the main focus of this work, has been reported by several groups.[7,14,47] Besides, we also observe an increase of τ_{eff} with the increase in T, as shown later in Section 4.5. These results are ascribable to T-dependent SRH recombination either in the bulk or at the surfaces according to the nature of the samples, and there is no precise model for simulating the T-dependence of SRH recombination. Therefore, for simplicity, we assume the single trap state located at the mid-gap level for calculating $\tau_{SRH,bulk}$ and τ_{surf}. We apply the standard SRH recombination model[48] for calculating $\tau_{SRH,bulk}$, while the recombination model for a-Si:H/c-Si interface proposed by Olibet et al[49] is applied for calculating R_{surf} and hence τ_{surf}. In the simulation, trap densities in the bulk (N_b) and at the a-Si:H/c-Si interface (N_s) are used as T-independent parameters to control bulk and surface SRH recombination. Other parameters used in this work is shown in Appendix A. For considering the effect of T dependence in SRH recombination, we herein assume an Arrhenius-type T dependence in hole capture cross sections (σ_p)[44] both for bulk and surface SRH recombination, with a constant activation energy (E_a).

4 | RESULTS AND DISCUSSION

4.1 | Bulk lifetime and surface recombination velocity

As explained in Section 2.1, we prepared two groups of SHJ solar cells with the same process condition except for the PECVD growth of (i)a-Si:H layers: Group A based on our standard condition and Group B (only three samples) with poorer surface passivation. The difference in surface passivation can be characterized by using Equation 2, since we prepared a series of SHJ cells with a wide range of w. Figure 2 shows the relationship between $1/w$ and $1/\tau_{eff}$ for the SHJ cells in both of the groups. The τ_{eff} measurement for this plot was performed after ITO deposition followed by the post annealing. From this plot and Equation 2, we obtain $\tau_{bulk} = 15$ ms and $S_{mean} = 1.1$ cm·s^{-1} for Group A. The same procedure was also applied for Group B, and we obtain $S_{mean} = 8.8$ cm·s^{-1}, which is eight times higher than that of Group A. Thus, it is confirmed that surface passivation in the SHJ cells is well controlled by modifying the PECVD condition, as expected.

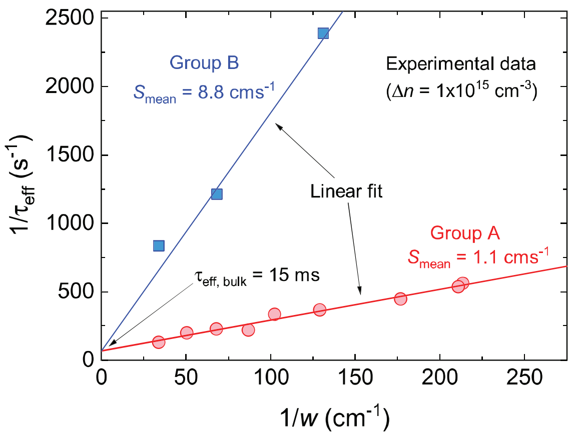

FIGURE 2 Relationship between the inverse of the wafer thickness w and the inverse of the effective lifetime τ_{eff} of the SHJ solar cells at an excess carrier density of $\Delta n = 1 \times 10^{15}$ cm^{-3}. The difference between groups A (circle) and B (square) is the PECVD condition for the growth of (i)a-Si:H layers; that is, surface passivation in Group B is intentionally controlled to be worse than the other [Colour figure can be viewed at wileyonlinelibrary.com]

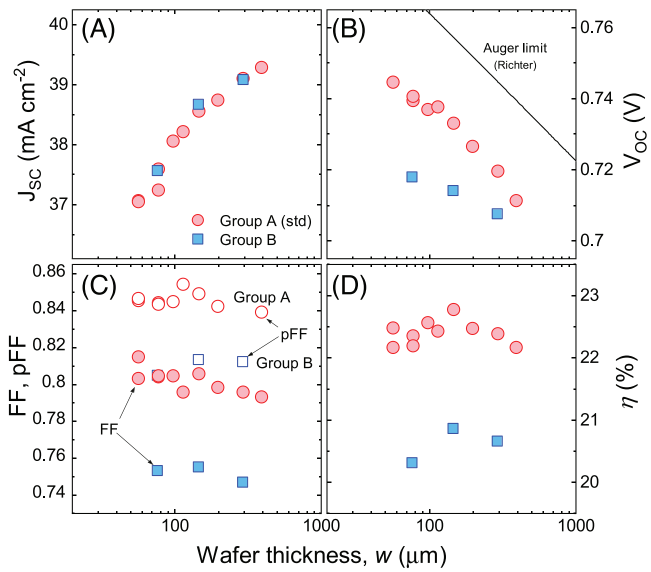

FIGURE 3 *J-V* characteristics of the SHJ solar cells fabricated in this study as a function of the wafer thickness measured under the STC conditions: (A) J_{SC}, (B) V_{OC}, (C) FF and pFF, and (D) η. The only difference between groups A (circle) and B (square) is the PECVD condition for the growth of (i)a-Si:H layers; that is, surface passivation in Group B is intentionally controlled to be worse than the other. The solid line in (B) shows the Auger limit calculated using Richter parameterization[42] [Colour figure can be viewed at wileyonlinelibrary.com]

4.2 | Photovoltaic properties of SHJ solar cells at STCs

Figure 3 shows the *J-V* characteristics of the SHJ solar cells fabricated in this study as a function of w, which were measured under STC. As shown in Figure 3A, both of groups A (standard condition) and B (poorer surface passivation) show the same trend in J_{SC}; the J_{SC} decreases monotonically from 39.5 to 37 mA·cm^{-2} by reducing w from 400 to 50 μm mainly due to the volume reduction of the Si absorber. In contrast, a clear difference between groups A and B is found in V_{OC} as shown in Figure 3B. In case of Group A, the V_{OC} increases logarithmically from 0.711 to 0.750 V with the decrease in w, while that of Group B is limited below 0.720 V and its w dependence is rather minor. It is also found that the w dependence of the V_{OC} in Group A agrees well with that of the Auger limit (solid line in Figure 3B), which suggests that Auger recombination dominates the entire recombination process under the open-circuit condition, although there still exist a discrepancy between them. This discrepancy is attributed to the insufficient surface passivation (S_{mean} is not zero) and the perimeter effect[50] since the area of our SHJ cells was small (4 cm^2). As shown in Figure 3C, large differences in the FF and pFF are also found between groups A and B across the samples. The difference in the pFF, which is solely attributed to the difference in surface passivation, increases with the decrease in w since the impact of surface recombination becomes more dominant for thinner cells.[19] The FF is affected also by the series resistance in addition to surface passivation. The gap between the pFF and FF (ΔFF = pFF − FF) of Group B is larger than that of Group A, indicating the larger series resistance due to the (i)a-Si:H layers. In addition, the ΔFF increases slightly with the increase in w regardless of the groups, which is attributable to the w-dependent resistive losses which originates from the increased J_{SC} and the increased series resistance due to wafer itself. A similar trend was also observed in the previous work.[19] The resulting η for Group A is distributed within a narrow range from 22.2% to 22.8% over the entire w range, with a broad maximum at around w = 150 μm, as shown in Figure 3D. Group B shows lower η by approximately 2% absolute than the other mainly due to the enhanced surface recombination.

The *J-V* parameters of some typical SHJ solar cells fabricated in this study are listed in Table 1. The best-efficiency cell in Group A gives η = 22.8% at w = 147 μm, which is higher by 2% absolute than that of Group B. The main differences are found in the V_{OC} and FF, as also seen in Figure 3. One of the thin SHJ cells in Group A (w = 56.5 μm) gives η = 22.4% without any additional antireflection coating. This is slightly improved from our previous work,[19] which is attributable to the improved surface passivation by modifying the wafer cleaning process and the PECVD conditions for the growth of (i)a-Si:H, and the process maturing. This sample was also independently measured by the Calibration, Standard, and Measurement Team in AIST. As shown in the bottom most line in Table 1, we obtained η = 22.7% with V_{OC} = 0.750 V, which is one of the highest efficiencies ever reported for very thin (w < 60 μm) Si wafers.

4.3 | Temperature coefficients

A typical temperature series of the *J-V* curves obtained in this study is shown in Figure 4. With the increase in T, the V_{OC} decreases largely while the J_{SC} increases slightly. Consequently, the output power

TABLE 1 Photovoltaic properties of SHJ solar cells prepared in this study measured under STC conditions

Surface passivation	Group	w µm	J_{SC} mA cm^{-2}	V_{OC} V	FF	Eff. %
Poor	B	146	38.7	0.708	0.759	20.8
Standard	A	147	38.5	0.733	0.806	22.8
Standard	A	56.5	37.1	0.747	0.810	22.4
Standard	A	56.5	37.27*	0.750*	0.814*	22.72*

Note: The cell area is 4 cm^2 designated by a shadow mask. Data with * symbols were independently measured by the Photovoltaic Calibration, Standards, and Measurement Team.

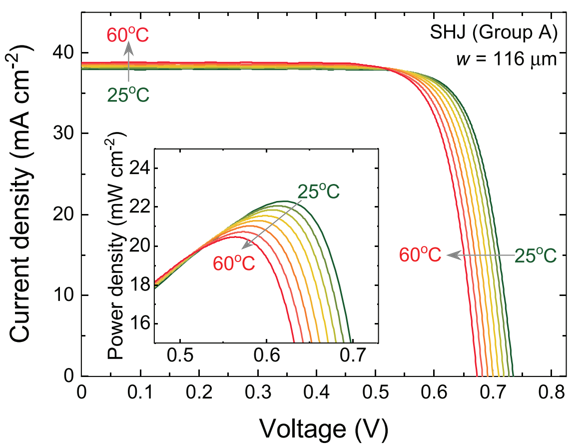

FIGURE 4 Measured temperature-dependence of the *J-V* curves of an SHJ solar cell (group A) fabricated in this study [Colour figure can be viewed at wileyonlinelibrary.com]

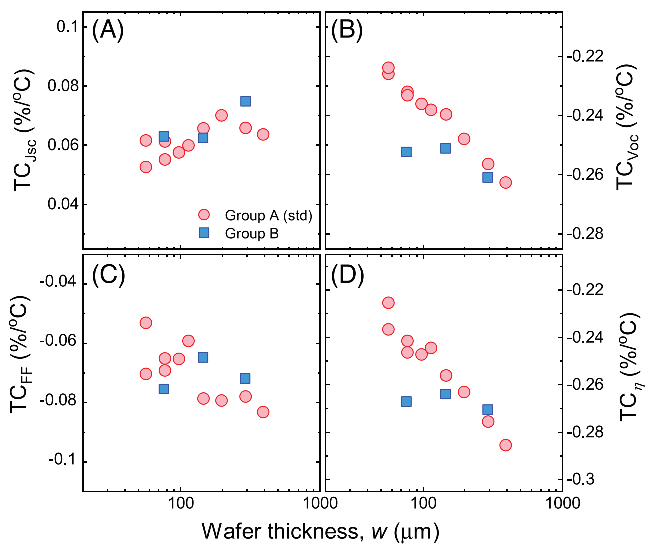

FIGURE 5 Temperature coefficients of the photovoltaic parameters in the SHJ solar cells shown in Figure 3: (A) TC_{JSC}, (B) TC_{VOC}, (C) TC_{FF}, and (D) TC_{η} [Colour figure can be viewed at wileyonlinelibrary.com]

density as well as the V_{MPP} decreases linearly with the increase in T, as shown in the inset.

The TC_{VOC}, TC_{JSC}, TC_{FF}, and TC_{η} obtained in this study are summarized in Figure 5, as a function of w. Note that only the TC_{JSC} takes positive values, whereas the others including the TC_{η} take negatives. As shown in Figure 5A, the TC_{JSC} is ranged from 0.05%/°C to 0.08%/°C mainly owing to the bandgap narrowing effect. The TC_{JSC} shows a slight increase with the increase in w, which suggests that dJ_{SC}/dT in Equation 4 is not constant across the samples. One of the possible reasons is the nonlinear T dependence of the absorption coefficients near E_g. However, detailed analysis remains as a future task. The positive coefficient of the TC_{JSC} is almost canceled by the TC_{FF}, which is ranged from −0.05%/°C to −0.08%/°C as shown in Figure 5C. In addition, no significant difference is observed between groups A and B for the TC_{JSC} and TC_{FF}. The larger data scattering in the TC_{FF} could be attributed to the less reproducibility of FF in our fabrication process. In contrast, the TC_{VOC} takes large negative values and shows a clear w dependence as shown in Figure 5B; the TC_{VOC} of Group A is improved from −0.26%/°C to −0.22%/°C monotonically by reducing w from 400 to 50 µm. However, such a w dependence in the TC_{VOC} is not clearly observed for Group B, which shows lower V_{OC} owing to the poor surface passivation. It is confirmed from Figures 3B and 5B that TC_{VOC} of a solar cell is improved by enhancing its V_{OC}, either via improving surface passivation or thinning the wafer. Consequently, the TC_{η} is dominated by the TC_{VOC} and is improved from −0.29%/°C to −0.22%/°C by thinning the wafer in case that surface passivation is sufficiently good (Group A), as shown in Figure 5D.

The correlation between the V_{OC} and the TC_{VOC} is summarized in Figure 6. In this figure, the TC_{VOC}s of the SHJ cells obtained in this study are plotted as a function of the V_{OC} at STC. For comparison, the TC_{VOC}s of c-Si cells with SHJ and other architectures in the previous reports[7,14,51,52] are also plotted in this figure, with an empirical fitting curve reported by Hishikawa et al.[53] It is found that the SHJ architecture shows superior TC_{VOC} owing to high V_{OC}, which originates from its superior surface passivation. Besides, the TC_{VOC} obtained in this study is improved further by thinning the wafer. Overall, all the experimental data follows the curve reported by Hishikawa et al, though all of our results are distributed slightly below the curve. Thus, enhancing the V_{OC} is crucial for improving the TC_{VOC} and hence the TC_{η}.

4.4 | Optimum thickness at high temperatures

In the previous subsection, we showed that the TC_{η} is improved by enhancing the V_{OC}, via either improving surface passivation or

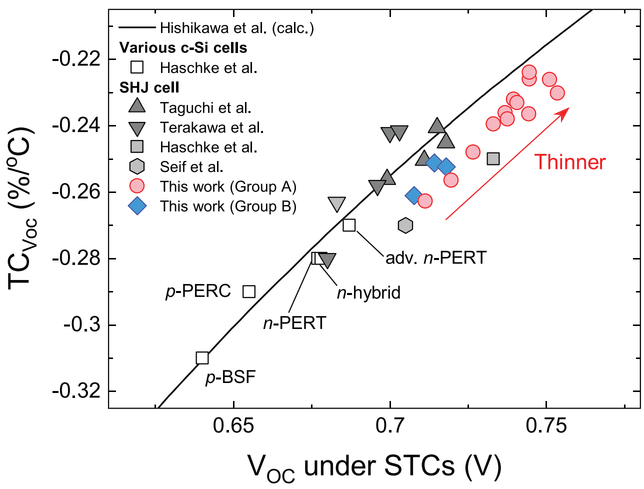

FIGURE 6 Correlation between the V_{OC} under STCs and the TC_{VOC} obtained in this study.[7,14,51,52] For comparison, data from the literatures are also plotted. BSF, PERC, and PERT are abbreviations for back surface field, passivated emitter rear cell, and passivated emitter rear totally diffused. The solid line is an empirical fit proposed by Hishikawa et al., $TC_{VOC} = \frac{1}{T}(1 - 1.232/V_{OC})^{53}$ [Colour figure can be viewed at wileyonlinelibrary.com]

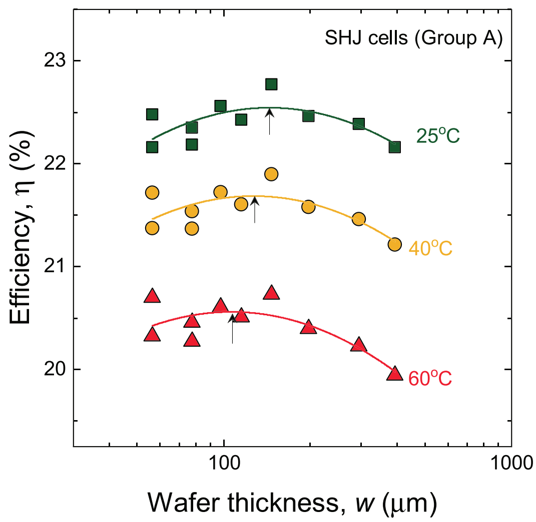

FIGURE 7 Conversion efficiencies of the SHJ solar cells at 25°C, 40°C, and 60°C as a function of the wafer thickness w. The solid curves are the polynomial fits to the measured data points. The small black arrows indicate the maximum points of the solid curves [Colour figure can be viewed at wileyonlinelibrary.com]

thinning the wafer. However, the most important parameter for increasing energy yield is not the TC_η but the absolute value of the η at operating conditions. As already stated in the introduction, the optimum w is determined by the trade-off between the V_{OC} and the J_{SC}, and it is approximately 98–110 μm at the standard testing temperature (25°C) for an ideal c-Si cell.[23,24] In the real c-Si cells, there are several optical losses owing to the surface reflection and the parasitic absorption within the supporting layers (e.g., ITO) and highly doped layers, resulting in the reduction in the J_{SC} particularly for thin c-Si cells. In addition, surface SRH recombination is not completely suppressed. Accordingly, the optimum wafer thickness of the real c-Si cells becomes thicker than that in the ideal case. In fact, as shown in Figure 3D, the highest η is obtained at $w = 140$ μm in the SHJ solar cells fabricated in this study (Group A). However, the optimum w is expected to become thinner with the increase in T, since the TC_{VOC} and hence the TC_η is improved with the increase in the V_{OC}, as shown in Figure 6. To confirm this, the values of the measured η of the SHJ cells at $T = 25$°C, 40°C, and 60°C are compared as a function of w as shown in Figure 7. It is clearly found that the η decreases substantially with the increase in T regardless of w, mainly due to the drop in the V_{OC}. It is also noticeable that the decreasing rate of the η becomes smaller with the decrease in w, owing to the improved TC_η. However, the best-η cell at 25°C ($w = 140$ μm) is still the best even at $T = 60$°C, since the initial η of the cells with $w < 140$ μm obtained in this study is not high enough to surpass it in this temperature range. Nevertheless, the shift of the optimum w toward the left side (thinner wafers) with the increase in T is clearly observed by comparing the peak positions of the polynomial fits of the measured data (solid lines).

Figure 8 shows the optimum w taken from the polynomial fits to the measured η including the solid lines in Figure 7 as a function of T.

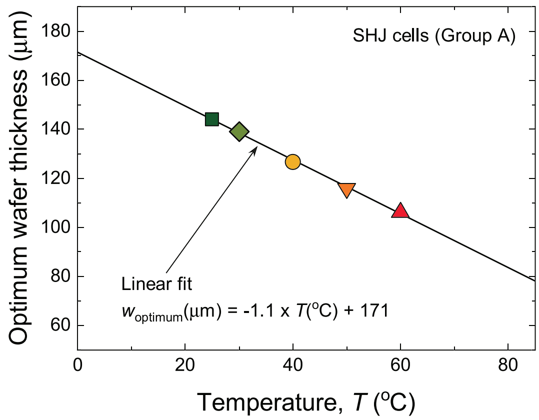

FIGURE 8 Correlation between the optimum wafer thickness and temperature. Each data point is determined from the polynomial fit of the measured data at each temperature. The solid line is a linear fit of the data points [Colour figure can be viewed at wileyonlinelibrary.com]

It is found that the optimum w decreases almost linearly with the increase in T. A linear fit of the data points gives the slope of -1.1 μm/°C and the intersection of 171 μm at 0°C. It should be noted that the results shown in Figure 8 was obtained based on our SHJ process, that has a large room for improvement in terms of η. In fact, the best efficiency SHJ cell reported so far shows an $\eta = 25.1$% with a V_{OC} of 0.747 V,[12] whereas the best η obtained in this work remains at 22.8% with a V_{OC} 0.733 V at $w = 147$ μm, as listed in Table 1. Therefore, the result shown in Figure 8 would shift downward, that is, toward thinner side, by improving the SHJ process including better surface passivation and so forth.

4.5 | Temperature dependence in ideal c-Si cells: Numerical simulation

In this subsection, the T-dependence in ideal c-Si cells are analyzed with the help of numerical simulation based on the method described in Section 3.2. First, we compare the simulated and the measured τ_{eff} at different temperatures. Figure 9A shows the simulated minority carrier lifetimes (τ_{int}, $\tau_{SRH,bulk}$, τ_{surf}, and τ_{eff}) assuming that SRH recombination parameters are constant. In this case, τ_{eff} decreases slightly with the increase in T. This originates from the enhanced SRH recombination owing to the increase in the thermal velocity of charge carriers. In contrast, the measured τ_{eff} shows a clear increase with temperature rising particularly for $\Delta n < 10^{15}$ cm^{-3} where SRH recombination is dominant.[7] This tendency can be reproduced quantitatively by introducing T dependent σ_p in SRH recombination, as shown in Figure 9B. In this case, we assume that σ_p for bulk and surface SRH recombination (σ_{bp} and $\sigma_{sp}{}^0$ in Appendix A) depend on T in an Arrhenius manner with $E_a = 0.1$ eV; that is, σ_p increases exponentially with $1/T$.[44] Thus, it is necessary to consider T dependence in SRH recombination parameters to reproduce the experimental results well. Nevertheless, its impact is not significant over the T range considered

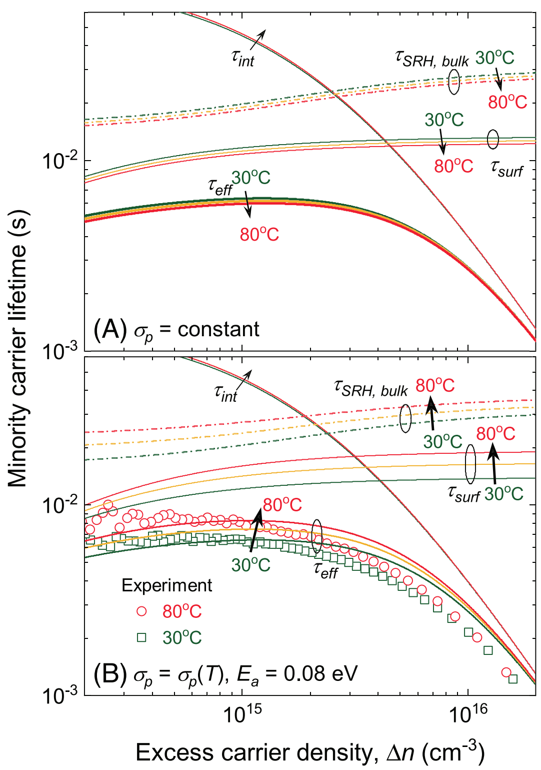

FIGURE 9 Comparison of the measured and simulated minority carrier lifetimes (τ_{int}, $\tau_{SRH,bulk}$, τ_{surf}, and τ_{eff}) as functions of excess carrier density for two cases: (A) all the SRH recombination parameters are independent of T, and (B) Arrhenius-type T dependence with $E_a = 0.1$ eV only for σ_p both in the bulk and at the interface. The measured τ_{eff} at 30°C and 80°C in (B) were obtained using an SHJ cell with $w = 146$ μm. $N_b = 2.9 \times 10^8$ cm^{-3} and $N_s = 2.4 \times 10^8$ cm^{-2} are used for the simulation

in this work ($\Delta\tau_{eff} = \sim+20\%$ at $\Delta n = 10^{15}$ cm^{-3} for $\Delta T = 60$°C), probably thanks to the high-quality Si wafers and excellent surface passivation at the a-Si:H/c-Si interface.

Figure 10 shows the T dependence of the implied efficiency $i\eta$ as a function of w. For simplicity, here we assume SRH recombination parameters are independent of T. The simulated temperature coefficient of $i\eta$, $TC_{i\eta}$, is also plotted for the right axis. In this figure, simulation was done for four different sets of N_b and N_s, and the corresponding $\tau_{SRH,bulk}$ and S are also noted inside the figure for comparison with the previous studies. As shown in Figure 10A, in case both of the bulk and surface defect densities are low, the maximum $i\eta > 29\%$ is achieved at $w \sim 100$ μm at 25°C, which agrees quantitatively with the previous report.[23,24] This efficiency is mostly limited by Auger recombination, as the τ_{eff} at the maximum power point (~7 ms for $w = 100$ μm) is dominated by τ_{Auger} (~9 ms) rather than $\tau_{SRH,bulk}$ or τ_{surf} (>30 ms). The maximum $i\eta$ decreases monotonically with the increase in T, which is mainly due to the reduction in the iV_{OC}. In addition, the optimum w that gives the maximum $i\eta$ shifts toward thinner side, because the reduction in w results in an increase in iV_{OC} and hence its temperature coefficient. For example, the maximum $i\eta$ at 80°C is obtained at $w \sim 30$ μm, which is rather thin compared to the current industrial standard (>150 μm). Consequently, $TC_{i\eta}$ improves from −0.29%/°C to −0.20%/°C by reducing w from 1000 to 10 μm. This result reveals that c-Si cells should be thinner for efficient power generation in hot and sunny regions, where the cell temperature easily reaches above 60°C.

The increase in defect densities, that is, the reduction in τ_{eff}, leads to the reduction of the maximum $i\eta$ and the $TC_{i\eta}$, as observed in Figure 10B–D, while the general trends observed in Figure 10A are also valid for these cases. Besides, it is also found from the comparisons of Figure 10A–D that the $TC_{i\eta}$ becomes less dependent on w, with the increase in the surface trap density, that is, S.

The impact of T on the optimum w is more clearly seen in Figure 11. In this figure, the optimum w is plotted as a function of T. The optimum w decreases monotonically with the increase in T in all cases shown in this figure. However, the absolute value of the optimum w is varied by the relative impacts of bulk and surface recombination on the total recombination. The increase in $\tau_{SRH,bulk}$ results in the upward shift of the curve, leading to the increase of the optimum w over the entire temperature range. This is explained by the increase of the relative impact of surface recombination on the total recombination. At the same time, the slope of the curve becomes steeper. In contrast, the reduction in S results in the downward shift of the curve, leading to the decrease of the optimum w. The experimental data shown in Figure 8 are also plotted in this figure for comparison. It is found that the experimental data follows the trend obtained by the simulation and are almost reproduced by the simulation using the experimentally determined parameters from Figure 2: $\tau_{SRH,bulk} = 15$ ms and $S = 1.1$ cm/s. This trend is maintained even if the T dependence of the σ_p for SRH recombination is considered, as shown in the thin dotted line in Figure 11, though the optimum w decreases slightly faster. Thus, it is clarified that thinning the wafer

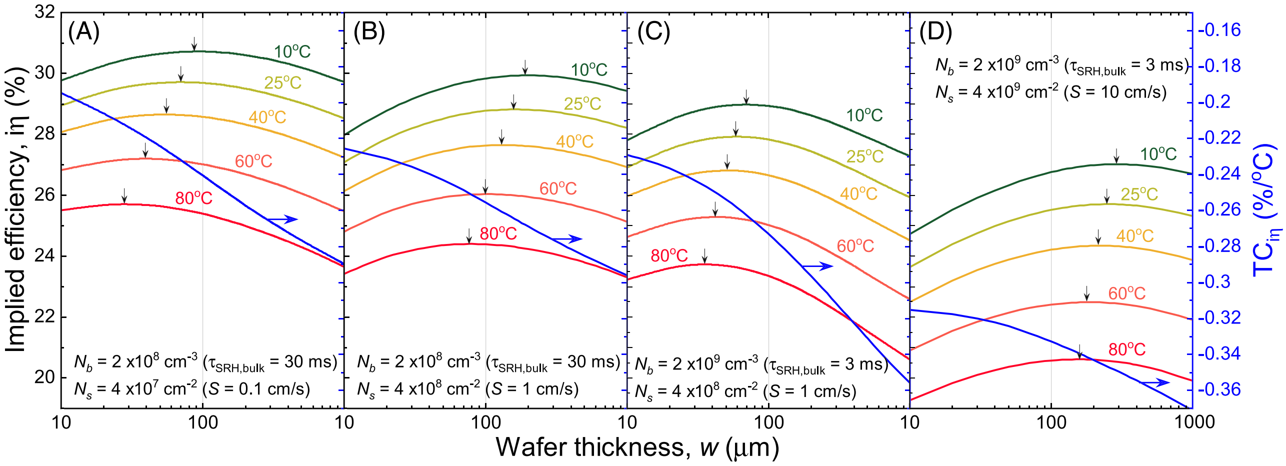

FIGURE 10 Simulated temperature-dependent implied efficiencies and temperature coefficients of c-Si solar cells. The defect densities (N_b and N_s) and the corresponding $\tau_{SRH,bulk}$ and S at $\Delta n = 10^{15}$ cm^{-3} and 25°C used in the simulation are noted inside the figures. The black arrows in the figure indicate the maximum efficiency point at each condition [Colour figure can be viewed at wileyonlinelibrary.com]

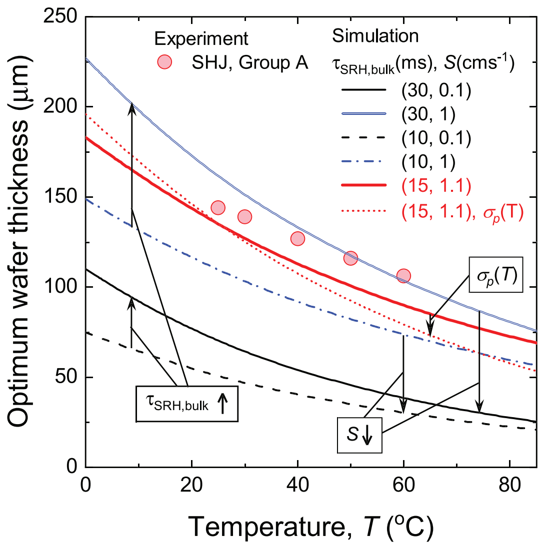

FIGURE 11 Correlation between the optimum wafer thickness and temperature obtained by simulation. The experimental data are replotted from Figure 8. In this simulation, we assume that SRH recombination parameters are constant, except the thin dotted line in which σ_p has an Arrhenius-type T dependence as shown in Figure 9B [Colour figure can be viewed at wileyonlinelibrary.com]

is effective to achieve higher absolute efficiencies as well as better temperature coefficients at high temperatures.

The results shown in Figure 11 is based on the lifetime simulation with Lambertian light trapping. As mentioned previously, there exist parasitic absorption losses in the actual SHJ solar cells owing to the supporting layers (a-Si:H, TCO, and metal layers), which reduce the J_{SC}. The effect of parasitic absorption becomes more pronounced with the decrease in w, resulting in an additional efficiency loss accompanied with thinning the wafer.[19] In such a condition, the optimum w is expected to be thicker than that of the ideal case. In fact, our experimental result in Figure 11 shows that the optimum w is slightly thicker and less T dependent than that of the ideal case. In other words, the optimum w is expected to be thinner by the further reduction of parasitic absorption loss, which is also crucial to enhance the absolute conversion efficiency of c-Si cells.

4.6 | Issues in simulation model

In this work, we compare the experimental results with numerical simulations in terms of the T dependence of the photovoltaic performance of c-Si solar cells. However, there are several issues which were not treated in this work. The most fundamental issue is the T dependence of recombination parameters. For example, Auger coefficients for Auger recombination are known to be T dependent, as reported by Altermatt et al.[41] Auger recombination is an intrinsic recombination process in c-Si so that this must be incorporated for more accurate modeling of ideal c-Si solar cells. In contrast, T dependence in SRH recombination parameters becomes more important to model realistic c-Si cells having various SRH recombination centers. In this work, we introduced the T-dependent σ_p to reproduce the experimental results in SHJ solar cells. Obviously, this is too simple to model a realistic SHJ solar cell. Further research is necessary to address this issue.

Apart from recombination, the T dependence of the series resistance in c-Si cells was also not considered in this work. In case of SHJ cells, it is known that the electrical conductivity of (i)a-Si:H thin films is enhanced with the increase in T. This positive effect mitigates the reduction in FF of SHJ solar cells at high temperatures.[7,14] The TC_{FF} of SHJ solar cells can be controlled by modifying the thickness and/or conductivity of (i)a-Si:H layers, which could lead to unusual behaviors of the TC_{FF} and hence the TC_η.[51,54] In contrast to a-Si:H, the conductivity of TCO and metal electrodes in general decreases with the increase in T owing to phonon scattering effect, which may cause an additional loss in FF at elevated temperature. These issues should be taken into account for more precise analysis in the device level, although their effects are supposed to be minor in our experiment.

5 | CONCLUSIONS

In this work, we investigated the impact of wafer thickness in c-Si solar cells from the viewpoint of the photovoltaic performance at high temperatures. We prepared and characterized a series of SHJ solar cells with a wide range of $w = 50–400$ μm, with conversion efficiencies of >22%. We confirmed experimentally that the V_{OC} of SHJ cells increases by thinning the Si wafer if surface recombination is sufficiently suppressed. As a result, a high V_{OC} of 0.75 V and an efficiency of 22.7% were attained in an SHJ cell with a thickness of 56 μm. We also found that the temperature coefficients of V_{OC} in SHJ cells is improved via thinning the wafer, owing to the V_{OC} enhancement effect. Accordingly, such thin SHJ cells show better temperature coefficient, that is, less efficiency degradation at elevated temperatures. In such a condition, the optimum wafer thickness for maximizing the efficiency becomes thinner with the increase in temperature, which is also reproduced by numerical simulation. The simulation predicted that the optimum thickness can be <50 μm at elevated temperatures (>60°C). This tendency is expected to be more emphasized as SRH recombination is suppressed more and the conversion efficiency becomes higher. These findings suggest that the choice of the wafer thickness is crucial in high-efficiency c-Si cells particularly for obtaining the maximum power generation in hot and sunny regions.

ACKNOWLEDGMENTS

The authors acknowledge T. Kawatsu and T. Nagai of Komatsu NTC Ltd. for preparing thin Si wafers and M. Tanabe for the technical support. This work was conducted under a project commissioned by the New Energy and Industrial Technology Development Organization (NEDO), Japan. A part of this work was conducted at the AIST Nano-Processing Facility, supported by "Nanotechnology Platform Program" of the Ministry of Education, Culture, Sports, Science and Technology (MEXT), Japan.

ORCID

Hitoshi Sai https://orcid.org/0000-0002-2938-551X
Takuya Matsui https://orcid.org/0000-0003-1589-7052

REFERENCES

1. IEA. (2020) Snapshot of Global PV Markets 2020. https://www.iea-pvps.org, 1–16.
2. Kurnik J, Jankovec M, Brecl K, Topic M. Outdoor testing of PV module temperature and performance under different mounting and operational conditions. *Sol. Energy Mater. Sol. Cells*. 2011;95(1):373-376.
3. Ye Z, Nobre A, Reindl T, Luther J, Reise C. On PV module temperatures in tropical regions. *Sol Energy*. 2013;88:80-87.
4. Kaldellis JK, Kapsali M, Kavadias KA. Temperature and wind speed impact on the efficiency of PV installations. Experience obtained from outdoor measurements in Greece. *Renew Energy*. 2014;66:612-624.
5. Usama Siddiqui M, Arif AFM, Kelley L, Dubowsky S. Three-dimensional thermal modeling of a photovoltaic module under varying conditions. *Sol Energy*. 2012;86(9):2620-2631.
6. Würfel P. Limitations on energy conversion in solar cells. In: *Physics of Solar cells*. 2nd ed. Weinheim: Wiley-VCH Verlag; 2009:181-182.
7. Seif JP, Krishnamani G, Demaurex B, Ballif C, De Wolf S. Amorphous/crystalline silicon interface passivation: Ambient-temperature dependence and implications for solar cell performance. *IEEE J Photovoltaics*. 2015;5(3):718-724.
8. Feldmann F, Simon M, Bivour M, Reichel C, Hermle M, Glunz SW. Carrier-selective contacts for Si solar cells. *Appl Phys Lett*. 2014; 104(18):181105.
9. Krügener J, Haase F, Rienäcker M, Brendel R, Osten HJ, Peibst R. Improvement of the SRH bulk lifetime upon formation of n-type POLO junctions for 25% efficient Si solar cells. *Sol. Energy Mater. Sol. Cells*. 2017;173:85-91.
10. Tanaka M, Taguchi M, Matsuyama T, et al. Development of new a-Si/c-Si heterojunction solar cells: ACJ-HIT (artificially constructed junction-heterojunction with intrinsic thin-layer). *Jpn J Appl Phys*. 1992;31(Part 1, No. 11):3518-3522.
11. Richter A, Müller R, Benick J, et al. Design rules for high-efficiency both-sides-contacted silicon solar cells with balanced charge carrier transport and recombination losses. *Nat Energy*. 2021;6(4):429-438.
12. Ru X, Qu M, Wang J, et al. 25.11% efficiency silicon heterojunction solar cell with low deposition rate intrinsic amorphous silicon buffer layers. *Sol. Energy Mater. Sol. Cells*. 2020;215:110643.
13. Mishima T, Taguchi M, Sakata H, Maruyama E. Development status of high-efficiency HIT solar cells. *Sol Energy Mater sol Cells*. 2011; 95(1):18-21.
14. Haschke J, Seif JP, Riesen Y, et al. The impact of silicon solar cell architecture and cell interconnection on energy yield in hot & sunny climates. *Energ Environ Sci*. 2017;10(5):1196-1206.
15. Steinkemper H, Geisemeyer I, Schubert MC, Warta W, Glunz SW. Temperature-dependent modeling of silicon solar cells-Eg, n i, recombination, and VOC. *IEEE J. Photovoltaics*. 2017;7(2):450-457.
16. Tohoda S, Fujishima D, Yano A, et al. Future directions for higher-efficiency HIT solar cells using a thin silicon wafer. *J Non Cryst Solids*. 2012;358(17):2219-2222.
17. Augusto A, Herasimenka SY, King RR, Bowden SG, Honsberg C. Analysis of the recombination mechanisms of a silicon solar cell with low bandgap-voltage offset. *J Appl Phys*. 2017;121(20):205704.
18. Sai H, Umishio H, Matsui T, et al. Impact of silicon wafer thickness on photovoltaic performance of crystalline silicon heterojunction solar cells. *Jpn J Appl Phys*. 2018;57(8S3):08RB10.
19. Sai H, Oku T, Sato Y, Tanabe M, Matsui T, Matsubara K. Potential of very thin and high-efficiency silicon heterojunction solar cells. *Prog Photovoltaics Res Appl*. 2019;27(12):1061-1070.
20. Balaji P, Dauksher WJ, Bowden SG, Augusto A. Improving surface passivation on very thin substrates for high efficiency silicon heterojunction solar cells. *Sol Energy Mater sol Cells*. 2020;216: 110715.
21. Taguchi M, Yano A, Tohoda S, et al. 24.7% record efficiency HIT solar cell on thin silicon wafer. *IEEE J. Photovoltaics*. 2014;4(1):96-99.
22. Danel, A, Harrison, S, Gerenton, F, et al. (2018) Silicon heterojunction solar cells with open-circuit-voltage above 750 mV. Proc. 35th EUPVSEC, 444–447.
23. Richter A, Hermle M, Glunz SW. Reassessment of the limiting efficiency for crystalline silicon solar cells. *IEEE J. Photovoltaics*. 2013; 3(4):1184-1191.
24. Schäfer S, Brendel R. Accurate calculation of the absorptance enhances efficiency limit of crystalline silicon solar cells with Lambertian light trapping. *IEEE J Photovoltaics*. 2018;8(4):1156-1158.
25. Augusto A, Karas J, Balaji P, Bowden SG, King RR. Exploring the practical efficiency limit of silicon solar cells using thin solar-grade substrates. *J Mater Chem a*. 2020;8(32):16599-16608.

26. Engelbrecht DA, Tiedje T. Temperature and intensity dependence of the limiting efficiency of silicon solar cells. *IEEE J Photovoltaics*. 2021;11(1):73-84.
27. Granata SN, Bearda T, Dross F, Gordon I, Poortmans J, Mertens R. Effect of an in-situ H2 plasma pretreatment on the minority carrier lifetime of a-Si:H(i) passivated crystalline silicon. *Energy Procedia*. 2012;27:412-418.
28. Sai H, Chen PW, Hsu HJ, Matsui T, Nunomura S, Matsubara K. Impact of intrinsic amorphous silicon bilayers in silicon heterojunction solar cells. *J Appl Phys*. 2018;124(10):103102.
29. Sai H, Hsu HJ, Chen PW, Chen PL, Matsui T. Intrinsic amorphous silicon bilayers for effective surface passivation in silicon heterojunction solar cells: a comparative study of interfacial layers. *Phys Status Solidi*. 2021;218:2000743.
30. Schroder DK. *Semiconductor Material and Device Characterization*. New York: Wiley-IEEE Press; 2015.
31. Sinton, R, and Cuevas, A (2000) A quasi-steady-state open-circuit voltage method for solar cell characterization. *16th Eur Photovolt Sol Energy Conf*, (May), 1152, 1-4.
32. Haschke J, Dupré O, Boccard M, Ballif C. Silicon heterojunction solar cells: recent technological development and practical aspects—from lab to industry. *Sol. Energy Mater. Sol. Cells*. 2018;187:140-153.
33. Green MA. Lambertian light trapping in textured solar cells and light-emitting diodes: analytical solutions. *Prog Photovoltaics Res Appl*. 2002;10(4):235-241.
34. Pässler R. Dispersion-related description of temperature dependencies of band gaps in semiconductors. *Phys Rev B - Condens Matter Mater Phys*. 2002;66(8):1-18.
35. Green MA. Intrinsic concentration, effective densities of states, and effective mass in silicon. *J Appl Phys*. 1990;67(6):2944-2954.
36. Green MA. Self-consistent optical parameters of intrinsic silicon at 300 K including temperature coefficients. *Sol Energy Mater sol Cells*. 2008;92(11):1305-1310.
37. Nguyen HT, Rougieux FE, Mitchell B, Macdonald D. Temperature dependence of the band-band absorption coefficient in crystalline silicon from photoluminescence. *J Appl Phys*. 2014;115(4):043710.
38. Couderc R, Amara M, Lemiti M. Reassessment of the intrinsic carrier density temperature dependence in crystalline silicon. *J Appl Phys*. 2014;115(9):093705.
39. Nguyen HT, Baker-Finch SC, Macdonald D. Temperature dependence of the radiative recombination coefficient in crystalline silicon from spectral photoluminescence. *Appl Phys Lett*. 2014;104(11):112105.
40. Trupke T, Green MA, Würfel P, et al. Temperature dependence of the radiative recombination coefficient of intrinsic crystalline silicon. *J Appl Phys*. 2003;94(8):4930-4937.
41. Altermatt PP, Schmidt J, Heiser G, Aberle AG. Assessment and parameterisation of Coulomb-enhanced Auger recombination coefficients in lowly injected crystalline silicon. *J Appl Phys*. 1997;82(10):4938-4944.
42. Richter A, Glunz SW, Werner F, Schmidt J, Cuevas A. Improved quantitative description of Auger recombination in crystalline silicon. *Phys Rev B - Condens Matter Mater Phys*. 2012;86(16):1-14.
43. Murphy JD, Bothe K, Krain R, Voronkov VV, Falster RJ. Parameterisation of injection-dependent lifetime measurements in semiconductors in terms of Shockley–Read–Hall statistics: an application to oxide precipitates in silicon. *J Appl Phys*. 2012;111(11):113709.
44. Schmidt J. Temperature- and injection-dependent lifetime spectroscopy for the characterization of defect centers in semiconductors. *Appl Phyics Lett*. 2003;82(13):2178-2180.
45. Paudyal BB, McIntosh KR, Macdonald DH. Temperature dependent carrier lifetime studies on Ti-doped multicrystalline silicon. *J Appl Phys*. 2009;105(12):124510.
46. Bernardini S, Naerland TU, Coletti G, Bertoni MI. Defect parameters contour mapping: a powerful tool for lifetime spectroscopy data analysis. *Phys Status Solidi*. 2018;255(8):1800082.
47. Vasudevan R, Poli I, Deligiannis D, Zeman M, Smets AHM. Temperature dependency of the silicon heterojunction lifetime model based on the amphoteric nature of dangling bonds. *AIP Adv*. 2016;6(11):115118.
48. Shockley W, Read WT. Statistics of the recombinations of holes and electrons. *Phys Rev*. 1952;87(5):835-842.
49. Olibet S, Vallat-Sauvain E, Ballif C. Model for a-Si:H/c-Si interface recombination based on the amphoteric nature of silicon dangling bonds. *Phys Rev B - Condens Matter Mater Phys*. 2007;76(3):1-14.
50. Haase F, Schafer S, Klamt C, et al. Perimeter recombination in 25%-efficient IBC solar cells with passivating POLO contacts for both polarities. *IEEE J. Photovoltaics*. 2018;8(1):23-29.
51. Taguchi M, Maruyama E, Tanaka M. Temperature dependence of amorphous/crystalline silicon heterojunction solar cells. *Jpn J Appl Phys*. 2008;47(2 PART 1):814-818.
52. Terakawa, A, Asaumi, T, Kobayashi, S, et al. (2005) High efficiency HIT solar cells and the effects of open circuit voltage on temperature coefficients. 15th Int. Photovoltaie Sci. Conf. Shanghai China 2005, 2.
53. Hishikawa Y, Doi T, Higa M, et al. Voltage-dependent temperature coefficient of the I-V curves of crystalline silicon photovoltaic modules. *IEEE J. Photovoltaics*. 2018;8(1):48-53.
54. Seif JP, Descoeudres A, Filipič M, et al. Amorphous silicon oxide window layers for high-efficiency silicon heterojunction solar cells. *J Appl Phys*. 2014;115(2):024502.

How to cite this article: Sai H, Sato Y, Oku T, Matsui T. Very thin crystalline silicon cells: A way to improve the photovoltaic performance at elevated temperatures. *Prog Photovolt Res Appl*. 2021;1–12. https://doi.org/10.1002/pip.3443

APPENDIX A: PARAMETERS FOR NUMERICAL SIMULATION USED IN THIS STUDY

All the simulations were done using these parameters, unless noted otherwise.

c-Si wafer		
Thickness	w	10–1000 μm
Resistivity (n-type)		2 Ωcm
Bulk SRH recombination		
Bulk trap density	N_b	10^8–10^{10} cm^{-3}
Capture cross section for electron	σ_{bn}	10^{-14} cm^2
Capture cross section for hole	σ_{bp}	10^{-14} cm^2
Surface SRH recombination		
Surface trap density	N_s	10^7–10^{10} cm^{-2}
Capture cross section of neutral states for electron	${\sigma_{sn}}^0$	5×10^{-18} cm^2
Capture cross section of neutral states for hole	${\sigma_{sp}}^0$	10^{-16} cm^2
Capture cross section of charged states for electron	${\sigma_{sn}}^+$	2.5×10^{-15} cm^2
Capture cross section of charged states for hole	${\sigma_{sp}}^-$	5×10^{-14} cm^2